Soft Matter

Accepted Manuscript

This is an *Accepted Manuscript*, which has been through the Royal Society of Chemistry peer review process and has been accepted for publication.

Accepted Manuscripts are published online shortly after acceptance, before technical editing, formatting and proof reading. Using this free service, authors can make their results available to the community, in citable form, before we publish the edited article. We will replace this *Accepted Manuscript* with the edited and formatted *Advance Article* as soon as it is available.

You can find more information about *Accepted Manuscripts* in the Information for Authors.

Please note that technical editing may introduce minor changes to the text and/or graphics, which may alter content. The journal's standard Terms & Conditions and the Ethical guidelines still apply. In no event shall the Royal Society of Chemistry be held responsible for any errors or omissions in this *Accepted Manuscript* or any consequences arising from the use of any information it contains.

ROYAL SOCIETY OF CHEMISTRY

www.rsc.org/softmatter

Journal Name RSCPublishing

ARTICLE

Protein-responsive assemblies from catechol-metal ion supramolecular coordination

Cite this: DOI: 10.1039/x0xx00000x

Received 00th January 2012,
Accepted 00th January 2012

DOI: 10.1039/x0xx00000x

www.rsc.org/

C. Yuan, [a] J. Chen, [b] S. Yu, [a] Y. Chang, [a] J. Mao, [a] Y. Xu, [c] W. Luo, [c] B. Zeng, [c] and L. Dai*[a, c]

Supramolecular self-assembly driven by catechol-metal ion coordination has gained great success in the fabrication of functional materials including adhesives, capsules, coatings and hydrogels. However, this route has encountered great challenge in the construction of nanoarchitectures in the absence of removable templates, because of the uncontrollable crosslinking of catechol-metal ion coordination. Herein, we show that a supramolecular approach, combining both catechol-metal ion coordination and polymer self-assembly together, can organize polymers into hybrid nanoassemblies ranging from solid particles, homogeneous vesicles to Janus vesicles. Without the introduction of specific binding ligand or complicated molecular design, these assemblies can totally disassemble in response to proteins. UV/vis absorption, fluorescence quenching and recovery investigations have confirmed that proteins can seize metal ions from the hybrid nanoassemblies, thus causing the degradation of catechol-metal ion coordination networks.

Introduction

Polymeric assemblies that are degradable in response to external stimuli have gained extensive attention due to their potential use in biomedical applications. The development of this research area depends to a large extent on the design and synthesis of building blocks with cleavable functionalities. Dynamic chemical interactions such as boronate, [1, 2] imine, [3, 4] disulfide bond [5-7] and metal-ligand coordination [8-11], that can be either incorporated into the polymer chains or used as cross-linker, are promising candidates for endowing assemblies with degradable features. Along with the cleavage of dynamic chemical interaction, polymer assemblies often exhibit smart behaviors including disassembly, permeability change and charge reversion. In comparison with the rapid stimuli-response caused by the change in physical property, chemical induced degradation usually carriers out in a slower and more controllable manner.

Small molecules or polymers with catechol functionality have high binding affinity to various surfaces including SiO_2, [12] Fe_3O_4 [13, 14] and some polymers. [15] With this feature, catechol functionalized polymers are attractive for the preparation of adhesives. [16-19] Notably, catechol-Fe^{3+} coordination has been developed into a reliable self-assembly driving force for the creation of degradable hydrogels [20, 21] and smart actuators. [22, 23] Also, three-dimensional (3D) networks derived from catechol-Fe^{3+} coordination have the ability to self-assemble on various surfaces ranging from nano-, micro- to macro-scale, thereby demonstrating significant implications in film fabrication and surface engineering. [24-26] However, self-assembly of polymers driven by catechol-Fe^{3+} coordination in solutions is often uncontrollable. Therefore, removable templates are needed for the fabrication of nano- or micro-sized catechol polymer-Fe^{3+} complex capsules. [25, 27]

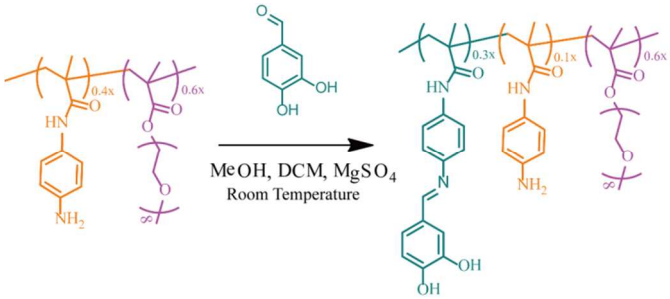

Scheme 1 Synthetic route of **CP** (M_n=12418, Đ=1.48) from P(APMA-co-MAPEG) (M_n=11806, Đ=1.51).

In this report, we show that a synergistic strategy, in which two driving forces *viz.* catechol-metal ion coordination and polymer self-assembly are combined together, can organize the catechol-metal ion coordination networks into nanoassemblies with tunable sizes and morphologies. The catechol functionality was incorporated onto the polymer chain through a Schiff base

formation reaction between poly (N-(4-aminophenyl)methacrylamide-co-polyethylene glycol monomethyl ether methacrylate) (P(APMA-co-MAPEG)) and 3, 4-dihydroxybenzaldehyde. This random copolymer was referred as **CP** (Scheme 1) and applied in the synergistic self-assembly approach to form **CP**-Fe^{3+} or **CP**-Cu^{2+} hybrid nanoassemblies. In addition to the tunable morphology, the as-formed nanoassemblies also have attractive protein-response feature. Proteins can competitively bind metal ions and induce the total disassembly of the hybrid nanoassemblies.

Results and discussion

Solid and vesicle-like hybrid assemblies

The feasibility of this synergistic approach was first tested by dissolving **CP** and metal compounds ($FeCl_3 \cdot 6H_2O$ or $CuCl_2 \cdot 2H_2O$) in two partially miscible solvents (water and *n*-butanol), separately. Since the solubility of water in *n*-butanol is ~16.3 vol% (at room temperature), when mixing these two solvents together with water content higher than this value, phase separation is readily formed (Fig. S6a). Interesting, although **CP** had a good solubility in both water and *n*-butanol, it could self-assemble in the water/*n*-butanol mixture and lead to the formation of stable emulsion (Fig. S6b-d). We envisaged that the emulsified solvent droplets might act as soft templates for the organization of catechol-metal ion coordination crosslinked networks, thus resulting in the formation of uniform nanoassemblies. Totally two feeding methods were adopted in this synergistic approach: (*i*) **CP**/water solution was injected into metal ion/*n*-butanol solution; (*ii*) metal ion/water solution was added into **CP**/*n*-butanol solution. Vigorous stirring was applied to ensure the fast mixing of two solutions.

In the case of injecting **CP**/water solution into $FeCl_3 \cdot 6H_2O$/*n*-butanol solution, **CP**-Fe^{3+} nanoassemblies prepared by using increased Fe^{3+} concentrations displayed an increase in particle size (Fig. 1a-c and the insets). All these assemblies regardless of their Fe^{3+} content were amorphous (electron diffraction patterns Fig. S7), implying that the absence of $FeCl_3$ crystals in the nanoassemblies. It should be noted that the molar ratios between catechol group and Fe^{3+} in these assemblies are ~3.8, ~1.9 and ~1.3. Thus, one Fe^{3+} coordinates with more than one catechol group to ensure the formation of cross-linked networks. This is understandable, as one Fe^{3+} can at most combine three catechol moieties. The coordination number of Fe^{3+} changes from 2, 4 to 6, depending on the concentration of catechol. [28, 29] Control experiments performed with a lower molar ratio of catechol to Fe^{3+} (such as 0.5) resulted in no nanoassemblies (Fig. S8a and c). Addition of Fe^{3+} into the **CP**-Fe^{3+} nanoassembly solution led to the disassembly of the particles (Fig. S8b and c). These were probably induced by the formation of mono complex, which prevented the formation of coordination cross-linked networks. The volume ratio between water and *n*-butanol unlikely had impact on the assembly morphology. Nanoassemblies prepared by adding 2.0, 4.0 and 6.0 mL of **CP**/water solutions into 10.0 mL of $FeCl_3 \cdot 6H_2O$/*n*-butanol solution had almost the same solid structure (Fig. 1d-f). These results indicated that only solid nanoassemblies could be formed when **CP**/water solution was injected into $FeCl_3 \cdot 6H_2O$/*n*-butanol solution. Dynamic light scattering (DLS) results tested in water solution (Fig.1g and h) indicated that all these solid assemblies had good monodispersities with polydispersities (PDI) ranging from 0.08-0.12. The stability of these solid assemblies was tested by tracking their size evolution under thermal-cycling in water solution. As shown in Fig. S9, the nanoassemblies shrunk-swelled slightly and reversibly with the cycling of temperature, which might be induced by the thermal-sensitivity of PEG chain .

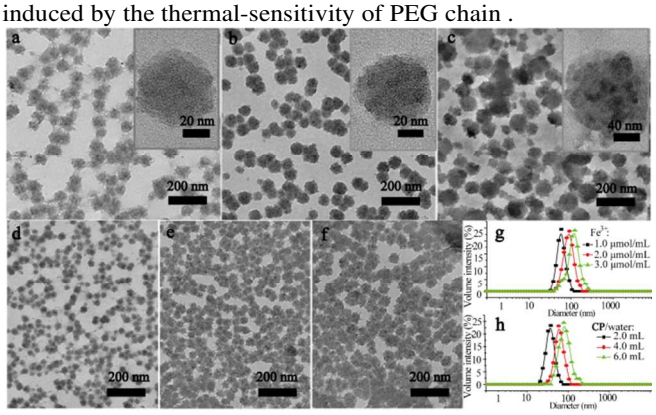

Fig. 1 Transmission electron microscope (TEM) images of **CP**-Fe^{3+} assemblies formed by injecting 5.0 mL of **CP**/water solution (~38.0 μmol catechol) into 10.0 mL of $FeCl_3 \cdot 6H_2O$/*n*-butanol solution with concentrations ranging from (a) 1.0, (b) 2.0 to (c) 3.0 μmol/mL. The insets of (a), (b) and (c) are magnified TEM images. TEM images of **CP**-Fe^{3+} assemblies prepared by injecting (d) 2.0, (e) 4.0 and (f) 6.0 mL of **CP**/water solutions (~38.0 μmol catechol) into 10.0 mL of $FeCl_3 \cdot 6H_2O$/*n*-butanol solution (2.0 μmol/mL). (g), (h) Diameters of the assemblies in water solution.

When injecting $FeCl_3 \cdot 6H_2O$/water solution into **CP**/*n*-butanol solution, nanoassemblies formed by using 2.0 and 4.0 mL of $FeCl_3 \cdot 6H_2O$/water solutions (Fig. 2a and b) were of solid morphology. Interesting, simply increasing the volume of $FeCl_3 \cdot 6H_2O$/water solution (6.0 or 8.0 mL) led to the formation of hollow vesicles (Fig. 2c and d). DLS results revealed that vesicles had larger particle size and PDI than that of solid assemblies (Fig. S10). The thermal-stability of the vesicles was almost the same with that of solid assemblies (Fig. S9). A typical scanning electron microscopy (SEM) image of a **CP**-Fe^{3+} vesicle was shown in the top-left of Fig. 2e, from which slightly shrunk surface could be observed. Importantly, the energy-dispersive X-ray spectroscopy (EDX) elemental mapping (Fe, C and N) of the vesicle shown in Fig. 2e clearly indicated the hollow structure. Small-angle X-ray scattering (SAXS) experiments further confirmed the multilamellar structure in the vesicle wall (Fig. 2f and g). Fitting to the lamellar form factor, [30, 31] the thickness of the multilamellar wall of the vesicles prepared by using 6.0 and 8.0 mL of water solutions were ~28.6 and ~34.2 nm, which fitted well with the results statistically analyzed from TEM images. The versatility of this synergistic self-assembly route has also been demonstrated by using Cu^{2+}. Like the **CP**-Fe^{3+} nanoassemblies, the feeding method also determined the morphology of the **CP**-

Cu^{2+} nanoassemblies. When injecting $CuCl_2 \cdot 2H_2O$/water solutions into **CP**/*n*-butanol solutions, **CP**-Cu^{2+} nanoassemblies changed from solid particles to hollow vesicles with the increasing volume of water solution (Fig. S11). Also, the morphology evolution was not observed when adding **CP**/water solutions into $CuCl_2 \cdot 2H_2O$/*n*-butanol solutions (Fig. S12).

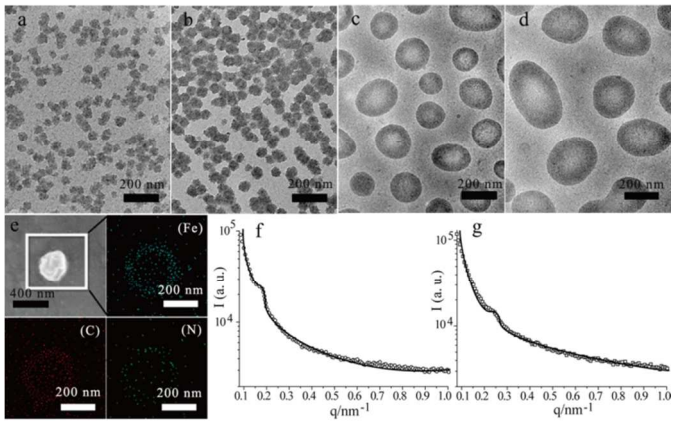

Fig. 2 TEM images of **CP**-Fe^{3+} assemblies prepared by injecting (a) 2.0, (b) 4.0, (c) 6.0 and (d) 8.0 mL of $FeCl_3 \cdot 6H_2O$/water solutions (containing 20 μmol of Fe^{3+}) into 10 mL of **CP**/*n*-butanol solution (5 mg/mL, ~38.0 μmol catechol group). (e) Typical SEM image of a **CP**-Fe^{3+} vesicle and EDX elemental mapping (Fe, C and N) of the vesicle. (f) And (g) are SAXS profiles of **CP**-Fe^{3+} vesicles formed by using 8.0 and 6.0 mL of $FeCl_3 \cdot 6H_2O$/water solutions.

To better understand the effect of feeding method on the morphology of the nanoassemblies, an assembly process was proposed in Scheme 2. As demonstrated in Fig. S6, with the presence of **CP**, stable emulsion could be formed if water solutions with volume ≥ 2.0 mL were injected into 10.0 mL of *n*-butanol solutions under stirring. DLS results indicated that the particle size of the droplets in these emulsions increased significantly with the increasing volume of water solution (Fig. S13). In these emulsions, metal compounds prefer water phase much more because of the ionization. In comparison, the migration of polymers from water into *n*-butanol is much slower, because of the chain entanglement. When injecting **CP**/water solution into metal compound/*n*-butanol solution, metal ions in the *n*-butanol phase can transfer fast into the **CP**/water droplets. This transfer speed may even be higher than the catechol-metal ion coordination reaction rate, and the coordination reaction between catechol and metal ions occurs in the whole **CP**/water droplet. Therefore, only solid nanoassemblies were formed regardless of the volume of **CP**/water solution (Scheme 2a).

In contrary, when adding metal compound/water solution into **CP**/*n*-butanol solution, the migration of polymer chains from *n*-butanol phase into water phase and the transfer of metal ions from water into *n*-butanol are much slower than the coordination reaction. Since the transfer speed of metal ions and **CP**, and the coordination reaction rate were constant, the morphology of the nanoassemblies was probably determined by the diameter of the emulsified water droplets. In the mixture with relatively lower water content, the water droplets were so small (Fig. S13) that **CP** could easily reach the core of the droplets. Thus, the coordination reaction was carried out in the whole droplet and led to the formation of solid assemblies. However, for the mixture with high water content, the as-formed water droplets were too large (Fig. S13) that **CP** could not reach the core of the droplet. As a result, catechol-metal ion complexes are mainly formed on the surface of water droplets, thereby leading to the formation of hollow vesicles (Scheme 2b). The evolution of UV/vis spectra during the formation of nanoassemblies confirmed the coordination between catechol and metal ions. **CP**-Fe^{3+} nanoassemblies showed evident absorptions at 248 and 335 nm (Fig. S14a), and **CP**-Cu^{2+} exhibited a characteristic absorption peak at 259 nm (Fig. S14b), which were different from the characteristic absorptions of **CP** (230 and 269 nm), Fe^{3+} (296 nm) and Cu^{2+} (lower than 200 nm). Thus, this synergistic approach is probably driven by both the polymer self-assembly and catechol-metal ion coordination.

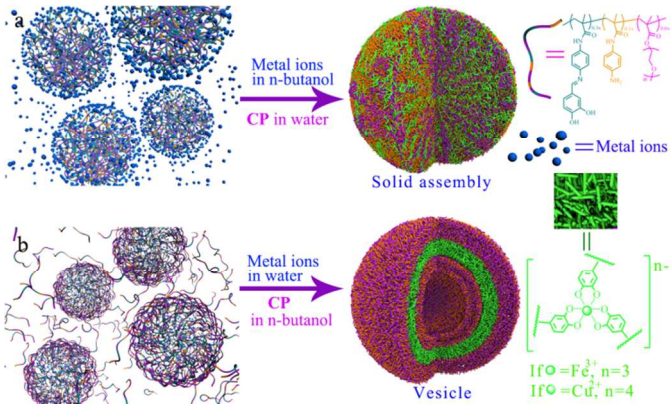

Scheme 2 Schematic illustration of the formation of solid and vesicle-like assemblies.

Janus hybrid vesicles

Based on the results above, it was clear that the formation of uniform **CP**-Fe^{3+} or **CP**-Cu^{2+} nanoassemblies benefited from the coordination reaction between catechol and metal ions in the heterogeneous system of water/*n*-butanol mixture. We were then interested in extending this approach to a heterogeneous system comprising two immiscible solvents (*viz.* hexane and water). To realize this self-assembly approach, $FeCl_3 \cdot 6H_2O$ was dispersed in hexane with the assistance of sonication and **CP** was dissolved in water. The coordination reaction was allowed to carry out undisturbedly on the interface of hexane and water solutions. Unexpectedly, Janus vesicles with dark domains embedded on the shells were formed (Fig. 3a-c). Increasing the concentrations of both $FeCl_3 \cdot 6H_2O$ and **CP** led to a significant increase in particle size (Fig. S15), but unlikely had influence on the morphology. SEM image shown in Fig. 3d revealed that the **CP**-Fe^{3+} Janus vesicles had asymmetric structure and shrunk slightly. EDX elemental mapping (Fe and C) clearly indicated that the shell thickness of the Janus vesicles were not homogenous (Fig. 3d). EDX line scan analysis further confirmed that the convex domain of the Janus vesicle contained evidently higher Fe element (Fig. 3e).

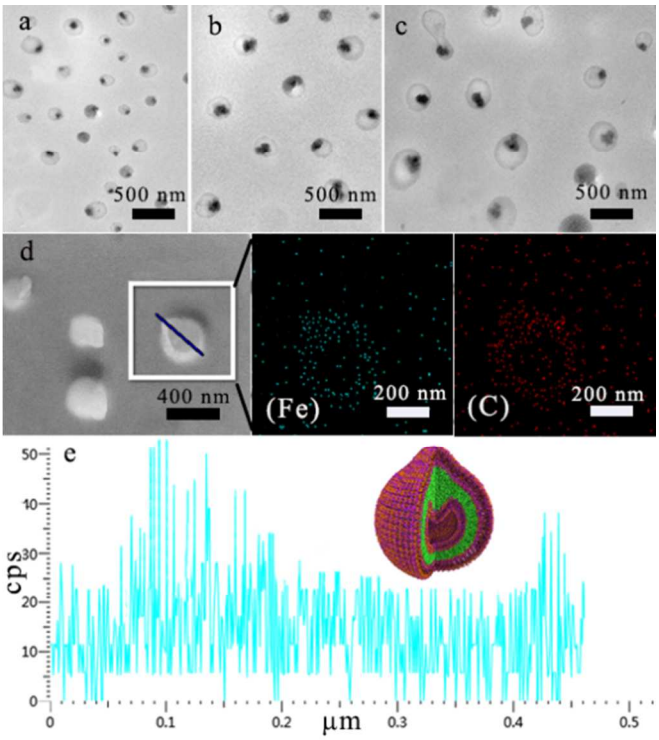

Fig. 3 TEM images of **CP**-Fe^{3+} Janus vesicles. From (a) to (c), the concentration of **CP** increases from 2.0, 4.0 to 6.0 mg/mL, while the corresponding concentration of $FeCl_3 \cdot 6H_2O$ ranges from 1.0, 2.0 to 3.0 μmol/mL. (d) Typical SEM image of **CP**-Fe^{3+} Janus vesicles and EDX elemental mapping (Fe and C) of the Janus vesicle. (e) EDX line scan (Fe) analysis of the Janus vesicle. The inset of (e) is the schematic illustration of Janus vesicle.

Since $FeCl_3 \cdot 6H_2O$ is insoluble in hexane, it can only be dispersed in this solvent to form a metastable suspension (Fig. S16). DLS results indicated that the diameter of $FeCl_3 \cdot 6H_2O$ nanocrystals in the suspension ranged from ~220 to ~640 nm, and increased evidently with the increasing content of $FeCl_3 \cdot 6H_2O$ (Fig. S16). On the other hand, **CP** can only stay in the water phase, as it is insoluble in hexane. Therefore, $FeCl_3 \cdot 6H_2O$ nanocrystals transfers quickly from hexane to water upon the contact of these two solutions. Once $FeCl_3 \cdot 6H_2O$ nanocrystals reach water phase, the coordination reaction between catechol and Fe^{3+} can be carried out on the surface of the nanocrystals to form a polymer shell. This crosslinked polymer shell can prevent the free **CP** in the water solution from contacting the encapsulated $FeCl_3 \cdot 6H_2O$ nanocrystals. With the further dissolution of $FeCl_3 \cdot 6H_2O$ nanocrystals, the as-released Fe^{3+} can only react with the pre-formed polymer shell by decreasing its coordination number. As a result, after the total dissolution and the completion of the coordination reaction, hollow Janus vesicles are formed.

Protein-triggered disassembly of hybrid assemblies

It is well known that a lot of proteins have high binding affinity to metal ions, almost one-third of all known proteins require metal ions for their structure and function. [32] Taking albumin from Bovine Serum (BSA) and trypsin as examples, they can coordinate with many metal ions such as Fe^{3+} and Cu^{2+}. The binding site of proteins depends on the species of both protein and metal ion. It has been confirmed that the binding center of BSA for Cu^{2+} is at Asp_1-Thr_2-His_3, [33] while for Fe^{3+} is at Trp_{135} and Trp_{214}. [34] Also, His_{143} and His_{151} have been recognized as the binding center of trypsin for Cu^{2+}. [35] Although the coordination between proteins and metal ions is a complicated process, their binding ability can be simply interpreted by using apparent stability constant (K_s). For BSA and trypsin binding to Fe^{3+} or Cu^{2+}, $Lg(K_s)$ is higher than 5.0. [36, 37] On the other hand, tris- and bis-catechol-Fe^{3+} complexes normally have high stability ($Lg(K_s) \approx 43$). [38, 39] However, this is not the case for **CP**, as measured by a fluorescence quenching method [40, 41], $Lg(K_s)$ for **CP**-Fe^{3+} is ~4.95, while for **CP**-Cu^{2+} is ~4.83 (Fig. S17). Possibly, the binding capability of ligands changes after attaching to polymer chains. [42, 43] For **CP**, the catechol functionality is rigidly attached to the polymer chain and the free rotation of this side group is barricaded, thereby inducing the decrease of binding affinity. Based on this result, we expected that BSA and trypsin might compete with **CP** in the binding of Fe^{3+} or Cu^{2+}, thus inducing the disassembly of **CP**-Fe^{3+} or **CP**-Cu^{2+} nanoassemblies.

The possibility of BSA and trypsin to coordinate with Fe^{3+} or Cu^{2+} was first confirmed by monitoring the evolution of UV/vis spectra. BSA, trypsin, Fe^{3+} and Cu^{2+} showed characteristic absorptions at 278, 280, 296 and lower than 200 nm, respectively (Fig. S18). BSA-Fe^{3+} complex showed absorption bands at 275 and 366 nm (Fig. S18a), while trypsin-Fe^{3+} complex had characteristic absorption peak at 284 nm (Fig. S18b). The absorption peaks of BSA-Cu^{2+} and trypsin-Cu^{2+} complexes appeared at 274 and 278 nm, respectively (Fig. S18c and d), which exhibited slightly blue-shift in comparison with BSA and trypsin. Addition of BSA or trypsin into the **CP** solution caused no change in absorption peaks (Fig. S19), suggesting that **CP** itself had no binding affinity to proteins. When BSA was added into the **CP**-Fe^{3+} nanoassembly solution, the absorption peaks derived from catechol-Fe^{3+} disappeared, while two new peaks at 275 and 350 nm arose (Fig. 4a). The peak intensity at 275 nm was enhanced evidently and the absorption at 350 nm shifted to 366 nm (attributed to BSA-Fe^{3+} complex) with the increasing concentration of BSA. This was probably induced by the increasing concentration of free **CP** and BSA-Fe^{3+} complex. When trypsin was added into the **CP**-Fe^{3+} nanoassembly solution, a new absorption peak appeared at 275 nm (Fig. 4b), which was lower than the characteristic peak of trypsin-Fe^{3+} complex (284 nm). Most likely, this new peak was a combination absorption of both free **CP** and trypsin-Fe^{3+} complex. In the case of **CP**-Cu^{2+} nanoassembly, the addition of BSA caused the emergence of a peak at 272 nm (Fig. 4c), which might be the combination absorption caused by free **CP** and BSA-Cu^{2+} complex. Similarly, this combined absorption peak of free **CP** and trypsin-Cu^{2+} complex was observed at 274 nm when trypsin was introduced into the **CP**-Cu^{2+} nanoassembly solution (Fig. 4d).

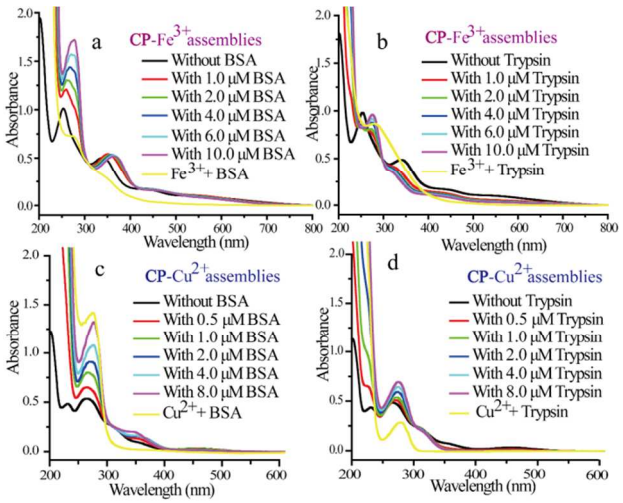

Fig. 4 UV/vis spectra of the nanoassemblies with the addition of proteins: (a) CP-Fe^{3+} assemblies with BSA, (b) CP-Fe^{3+} assemblies with trypsin, (c) CP-Cu^{2+} assemblies with BSA and (d) CP-Cu^{2+} assemblies with trypsin. All these spectra were measured at least 4.0 h after the addition of proteins to reach equilibrium states.

The particle size evolution of the nanoassemblies was monitored to further study the protein responsive behavior. Note that the UV/vis absorptions of the nanoassemblies changed upon the addition of proteins. But the disassembly of the nanoassemblies had critical concentration (*CC*) of protein. The protein concentration lower than *CC* only caused a slight swelling of the nanoassemblies, while protein concentration higher than *CC* induced the disassembly of nanoassemblies. It was observed that the *CC* value depended largely on the metal ion species and concentrations, and the protein species (Table S2 and S3). The disassembly kinetics of the nanoassemblies were tested using protein concentrations 2 folds of *CC*. The results shown in Fig. 5a-d indicated that: (*i*) these nanoassemblies adopted a total disassembly manner, as the final diameters of the particles in solutions after disassembly were consistent with that of the protein-metal ion complexes (Fig. S20, S21); (*ii*) solid nanoassemblies with high metal ion content and Janus vesicles swelled slightly before disassembly; (*iii*) the disassembly speed of nanoassemblies changed according to the order of Janus vesicles < solid assemblies with higher metal ion content < solid assemblies with lower metal ion content < vesicles; (*iv*) **CP**-Fe^{3+} assemblies disassembled more slowly than **CP**-Cu^{2+} assemblies when using the same protein; (*v*) BSA had a higher capability to trigger the disassembly of the nanoassemblies than trypsin. The swelling phenomenon of the nanoassemblies before disassembly could be explained by the absorption of proteins. This is possible because metal ions in the nanoassemblies with 2 or 4 coordination numbers can further bind proteins by increasing their coordination value. For **CP**-Fe^{3+} Janus vesicles, the dark domains possessed high content of Fe^{3+}, which could provide sufficient Fe^{3+} to bind proteins, thus postponing the disassembly behavior.

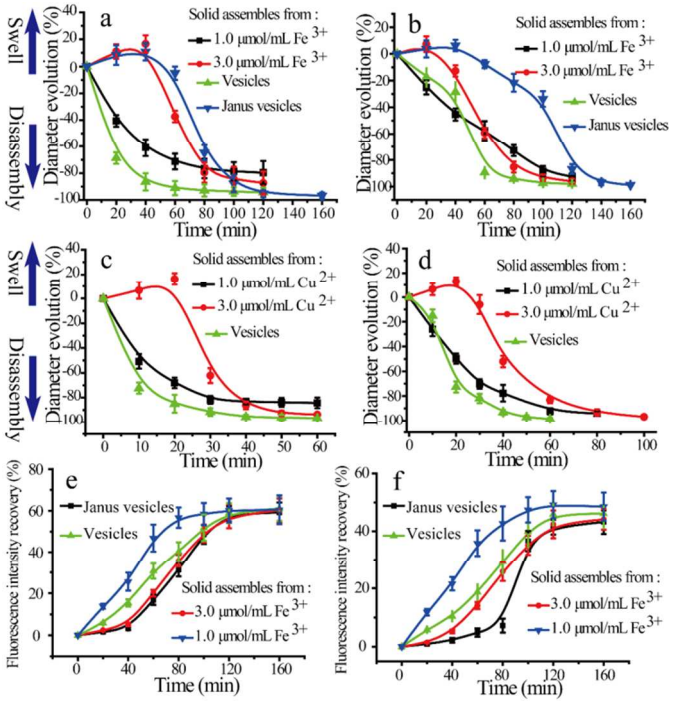

Fig. 5 Diameter evolutions of the nanoassemblies with the addition of proteins: (a) **CP**-Fe^{3+} assemblies with BSA, (b) **CP**-Fe^{3+} assemblies with trypsin, (c) **CP**-Cu^{2+} assemblies with BSA and (d) **CP**-Cu^{2+} assemblies with trypsin. Fluorescence intensity recovery kinetics of the **CP**-Fe^{3+} assemblies triggered by BSA (e) and trypsin (f) with concentrations 2 folds of *CC*. The vesicles and Janus vesicles used in these measurements were prepared by using 2.0 and 3.0 μmol/mL of $FeCl_3 \cdot 6H_2O$ solutions, respectively.

Since the binding of metal ions could cause the fluorescence quenching of **CP**, it was important to verify whether the protein-triggered disassembly of **CP**-Fe^{3+} and **CP**-Cu^{2+} nanoassemblies was accompanied with the fluorescence recovery of **CP**. This might provide deep insight into the fact that the disassembly event was induced by the competitive binding of metal ions between proteins and **CP**. Indeed, evident fluorescence recovery was observed after the addition of BSA or trypsin into the solutions of nanoassemblies (Fig. S22). However, the fluorescence of **CP** could not fully recovered even at high protein concentrations. The equilibrium fluorescence intensity recovery for systems **CP**-Fe^{3+}/BSA, **CP**-Fe^{3+}/trypsin, **CP**-Cu^{2+}/BSA and **CP**-Cu^{2+}/trypsin were calculated to be ~63.4, ~49.8, ~72.6 and ~58.6%. Also, the kinetics of fluorescence intensity recovery was monitored by taking **CP**-Fe^{3+} nanoassemblies as examples. The profiles of the fluorescence intensity recovery kinetics fitted well with the diameter evolution (Fig. 5e, f and Fig. S23). However, it should be noted that the **CP**-Fe^{3+} vesicles had lower fluorescence intensity recovery speed than the **CP**-Fe^{3+} solid assemblies derived from 1.0 μmol/mL of Fe^{3+}, which was different from the order of disassembly speed. This is understandable, as the fluorescence dequenching speed is determined by the content of Fe^{3+} in the nanoassemblies, while the vesicles could disassemble more easily. To this end, it is reasonable to consider that proteins can seize the metal ions from the nanoassemblies and induce a protein-triggered disassembly

(Scheme 3). This protein-triggered disassembly feature, driven by the competitive binding of metal ions, may be of great implication in biological applications, as the diseased tissue locations often exhibit variations in protein concentrations. [44, 45]

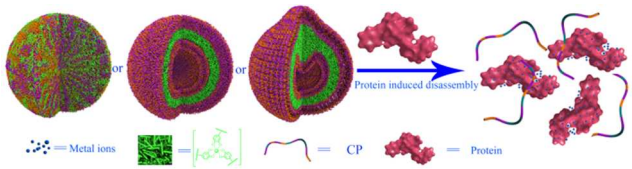

Scheme 3 Disassembly process of the hybrid assemblies triggered by protein.

Conclusions

In summary, we have outlined a synergistic route to polymer-metal hybrid architectures with tunable morphologies ranging from solid particles, homogeneous vesicles to Janus vesicles. By simply combining the driving forces of polymer self-assembly and catechol-metal ion coordination, this route can overcome the uncontrollable cross-linking and promote the self-organization of the polymer networks. In the viewpoint of methodology, this synergistic self-assembly route may be of great potential in the fabrication of hybrid nanovehicles with adjustable components and properties because of the designable functionality of the polymer. In comparison with traditional protein-sensitive nanovehicles, these nanoassemblies show apparent advantages including simple molecular design, total disassembly and tunable disassembly speed. When considering the residual amino group attached on the polymer chains, these nanoassemblies may be further decorated to realize more complicated functions. Additional work is also required to improve the specificity of the protein sensitivity and prolong the disassembly process.

Experimental

Materials

Methacryloyl chloride, 3, 4-dihydroxybenzaldehyde, triethylamine, *p*-phenylenediamine, magnesium sulfate anhydrous ($MgSO_4$), polyethylene glycol monomethyl ether methacrylate (PEGMA, M_W ~475), iron (III) chloride hexahydrate ($FeCl_3 \cdot 6H_2O$), copric chloride dihydrate ($CuCl_2 \cdot 2H_2O$), 2,2′-azobis(2-methylpropionitrile) (AIBN), albumin from Bovine Serum (BSA) and trypsin and other conventional reagents were obtained from commercial sources and were used as received.

Characterization

NMR spectra of synthetic monomer and resultant polymers in solutions were measured on a Bruker ARX 400MHz spectrometer. Molecular weights of the random copolymers were estimated by gel permeation chromatography (GPC) with a refractive index detector using THF as eluent (PMMA was used as standard). DLS measurements were performed on a Malvern Nanozetasizer. UV/vis absorption data of the samples were acquired in solutions by using UV spectrophotometry (Unico UV/vis 2802PCS). TEM measurements and electron diffraction experiment were performed with a JEM2100 at an acceleration voltage of 200 kV. SEM images were taken using a Hitachi SU-70 SEM instrument. Energy-dispersive X-ray spectroscopy (EDX) analyses were taken using an EDX attachment (INCA, Oxford Instruments) on the Hitachi SU-7 SEM instrument. The fluorescence emission spectra were measured by a FLS920 Fluorescence Lifetime and Steady State Spectrometer. Small-angle X-ray scattering (SAXS) was taken on Anton Paar SAXSess mc^2 by filling the specific quartz capillary with the solutions of the nanoassemblies, using Cu Kα (λ = 1.54184 Å, 40 kV, 50 mA) X-ray sources at room temperature.

Methods

Synthesis of N-(4-aminophenyl)methacrylamide (APMA): Methacryloyl chloride (2.19 g, 21.0 mM) and *p*-phenylenediamine (2.16 g, 20.0 mM) were dissolved in 10 mL and 50 mL of dichloromethane (DCM), respectively. Triethylamine (2.2 g, 22.0 mM) was added to the solution of *p*-phenylenediamine. Then, methacryloyl chloride DCM solution was added dropwise into the *p*-phenylenediamine solution at 5 ^oC. After stirring at room temperature for 12 h, the reaction mixture was washed with NaOH solution two times and with water three times to reach a neutral pH. The oil phase containing the key product was collected and dried with efficient $MgSO_4$. The crude product was obtained after the removal of solvent by rotary evaporation. The pure product was purified by passing through a column chromatography using silica gel as stationary phase and mixture of ethyl acetate/hexane (2:1) with 2.0 vol% triethylamine as eluent. Yield: 58 %. ^1H NMR (400 MHz, DMSO-D6) δ (ppm): 9.35 (s, 1H), 7.27 (d, 2H), 6.50 (d, 2H), 5.72 (s, 1H), 5.41 (s, 1H), 4.87 (s, 2H), 1.93 (s, 3H); ^{13}C NMR (300 MHz, DMSO-D6) δ (ppm): 166.41, 145.48, 141.12, 128.3, 122.53, 119.42, 114.07, 19.32.

Synthesis of P(APMA-co-MAPEG): To a 10.0 mL Schlenk tube, was charged 0.176 g APMA (1.0 mmol), 0.95 g MAPEG (2.0 mmol), 15.0 mg AIBN (0.09 mmol) and 5.0 mL tetrahydrofuran (THF). Three freeze-pump-thaw cycles were performed to eliminate the oxygen in the reaction mixture. After 24 h polymerization at 70 ^oC in argon atmosphere, the obtained product was purified by dissolving in THF and precipitating in hexane for three times. Pure product was obtained by drying at room temperature in vacuum for 24.0 h.

*Incorporation of catechol functionality onto P(APMA-co-MAPEG) to form **CP** multi-component random copolymer:* 0.5 g of P(APMA-co-MAPEG) was dissolved in 10.0 mL of dichloromethane solution followed by the addition of 2.0 g of $MgSO_4$. To this mixture, 0.035 g of 3, 4-dihydroxybenzaldehyde (0.25 mmol) in 2 mL of methanol solution was added dropwise. After 6 h reaction at room temperature under vigorous stirring, the solid precipitate in the reaction mixture was eliminated by filtration. The solution was

concentrated by rotary evaporation to give crude product. Then, purified CP was obtained by dissolving the crude product in THF and precipitating in hexane for three times.

*Self-assembly of **CP** driven by catechol-metal ion coordination:* Three different methods were adopted to control the morphology of the resultant assembly. (*i*) Preparation of solid assemblies. **CP** (50.0 mg, the content of catechol functionality was calculated to be about 38.0 μmol) was dissolved in water. Metal compounds ($FeCl_3 \cdot 6H_2O$ or $CuCl_2 \cdot 2H_2O$) were dissolved in *n*-butanol to form solutions with various concentrations. After the injection of polymer solutions into the metal compound solutions under stirring, solid spherical assemblies were obtained. (*ii*) For the preparation of vesicles, metal compounds ($FeCl_3 \cdot 6H_2O$ or $CuCl_2 \cdot 2H_2O$) were dissolved in water, while **CP** (50.0 mg) was dissolved in *n*-butanol. Metal compound solutions were injected into the **CP** solutions under stirring treatment to form vesicles. (*iii*) To prepare nanoassemblies with Janus morphology, hexane was used as solvent to disperse $FeCl_3 \cdot 6H_2O$. Although $FeCl_3 \cdot 6H_2O$ is insoluble in hexane, it can be dispersed in hexane to form metastable mixtures with the sonication treatment. The dispersion of metal compound in hexane was gently added to the **CP** water solution (containing 50.0 mg polymer) to form double-layered reaction system. The interfacial reaction was allowed to carry out undisturbedly to give Janus assemblies.

Acknowledgements

This work was supported by the National Natural Science Foundation of China (51373142, U1205113); Xiamen Science and Technology Committee (No. 3502Z20133003).

Notes and references

[a] College of Materials, Xiamen University, Xiamen, 361005, China.
[b] College of Chemistry and Chemical Engineering, Xiamen University, Xiamen, 361005, China.
[c] Fujian Provincial Key Laboratory of Fire Retardant Materials, College of Materials, Xiamen University, Xiamen, 361005, China. E-mail: lzdai@xmu.edu.cn

† Electronic Supplementary Information (ESI) available: Synthetic and characterization details, NMR spectra, TEM images, DLS results, UV/vis spectra and fluorescent spectra of the resultant products. See DOI: 10.1039/b000000x/

1 Y. Li, W. Xiao, K. Xiao, L. Berti, J. Luo, H. P. Tseng, G. Fung and K. S. Lam, *Angew. Chem. Int. Ed.*, 2012, **51**, 2864-2869.
2 K. T. Kim, J. J. L. M. Cornelissen, R. J. M. Nolte and J. C. M. van Hest, *J. Am. Chem. Soc.*, 2009, **131**, 13908–13909.
3 J. Gu, W. P. Cheng, J. Liu, S. Y. Lo, D. Smith, X. Qu, Z. Yang, Biomacromolecules, 2008, **9**, 255-262.
4 R. M. Sawant, J. P. Hurley, S. Salmaso, A. Kale, E. Tolcheva, T. S. Levchenko, V. P. Torchilin, *Bioconjugate Chem.*, 2006, **17**, 943-949.
5 D. C. González-Toro, J. -H. Ryu, R. T. Chacko, J. Zhuang and S. Thayumanavan, *J. Am. Chem. Soc.*, 2012, **134**, 6964–6967.
6 J. Li, M. Huo, J. Wang, J. Zhou, J. M. Mohammad, Y. Zhang, Q. Zhu and A. Y. Waddad, Q. Zhang, *Biomaterials*, 2012, **33**, 2310-2320.
7 S. Singh, F. Topuz, K. Hahn, K. Albrecht and J. Groll, *Angew. Chem. Int. Ed.*, 2013, **52**, 3000-3003.
8 H. Hofmeier, R. Hoogenboom, M. E. L. Wouters and U. S. Schubert, *J. Am. Chem. Soc.*, 2005, **127**, 2913-2921.
9 Rudy J. Wojtecki, Michael A. Meador and S. J. Rowan, *Nat. Mater.*, 2011, **10**, 14-27.
10 T. R. Cook, Y. -R. Zheng and P. J. Stang, *Chem. Rev.*, 2013, **113**, 734-77.
11 F. Wang, J. Zhang, X. Ding, S. Dong, M. Liu, B. Zheng, S. Li, L. Wu, Y. Yu, H. W. Gibson and F. Huang, *Angew. Chem.*, 2010, **122**, 1108-1112.
12 S. A. Mian, X. Gao, S. Nagase and J. Jang, *Theor. Chem. Acc.* 2011, **130**, 333-339.
13 E. Amstad, T. Gillich, I. Bilecka, M. Textor and E. Reimhult, *Nano Lett.*, 2009, **9**, 4042-4048.
14 E. Amstad, A. U. Gehring, H. Fischer, V. V. Nagaiyanallur, G. Hähner, M. Textor and E. Reimhult, *J. Phys. Chem. C*, 2011, **115**, 683-691.
15 H. Lee, S. M. Dellatore, W. M. Miller and P. B. Messersmith, *Science*, 2007, **318**, 426-430.
16 H. Lee, B. P. Lee and P. B. Messersmith, *Nature*, 2007, **448**, 338-342.
17 Y. Liu, K. Ai and L. Lu, *Chem. Rev*., 2014, **114**, 5057-5115.
18 S. Moulay, *Polymer Reviews*, 2014, **54**, 436-513.
19 B. K. Ahn, D. W. Lee, J. N. Israelachvili and J. H. Waite, *Nat. Mater.*, 2014, **13**, 867-872.
20 N. Holten-Andersena, M. J. Harringtonb, H. Birkedalc, B. P. Leed, P. B. Messersmithd, K. Y. C. Leea and J. H. Waite, *PNAS*, 2011, **108**, 2651-2655.
21 D. G. Barrett, D. E. Fullenkamp, L. He, N. Holten-Andersen, K. Y. C. Lee and P. B. Messersmith, *Adv. Funct. Mater*., 2013, **23**, 1111-1119.
22 B. P. Leea, M. -H. Lin, A. Narkar, S. Konst and R. Wilharm, *Sensors and Actuators B: Chemical*, 2015, **206**, 456-462.
23 B. P. Lee and S. Konst, *Adv. Mater.*, 2014, **26**, 3415-3419.
24 S. M. Kang, I. You, W. K. Cho, H. K. Shon, T. G. Lee, I. S. Choi, J. M. Karp and H. Lee, *Angew. Chem. Int. Ed.*, 2010, **49**, 9401-9404.
25 H. Ejima, J. J. Richardson, K. Liang, J. P. Best, M. P. van Koeverden, G. K. Such, J. Cui and F. Caruso, *Science*, 2013, **341**, 154-157.
26 J. Cui, Y. Ju, K. Liang, H. Ejima, S. Lörcher, K. T. Gause, J. J. Richardson and F. Caruso, *Soft Matter*, 2014, **10**, 2656-2663.
27 J. Guo, Y. Ping, H. Ejima, K. Alt, M. Meissner, J. J. Richardson, Y. Yan, K. Peter, D. von Elverfeldt, C. E. Hagemeyer and F. Caruso, *Angew. Chem. Int. Ed.*, 2014, **53**, 5546-5551.
28 S. W. Taylor, D. B. Chase, M. H. Emptage, M.J. Nelson and J. H. Waite, *Inorg. Chem.*, 1996, **35**, 7572-7577.
29 H. Zenga, D. S. Hwang, J. N. Israelachvilib and J. H. Waite, *PANS*, 2010, **107**, 12850-12853.
30 S. Förster, A. Timmann, C. Schellbach, A. Frömsdorf, A. Kornowski, H. Weller, S. Roth and P. Lindner, *Nat. Mater.*, 2007, **6**, 888-893.
31 R. Rodríguez-García, M. Mell, I. López-Montero, J. Netzel, T. Hellweg and F. Monroy, *Soft Matter*, 2011, **7**, 1532-1542.
32 J. A. Ibers and R. H. Holm, *Science*, 1980, **209**, 223-235.
33 H. Liang, B. Xin, X. Wang, Y. Yuan, Y. Zhou and P. Shen, *Chin. Sci. Bull.*, 1998, **43**, 404-409.

34 X. Xu, L. Zhang, D. Shen, H. Wu and Q. Liu, *J. Fluoresc.*, 2008, **18**, 193-201.
35 L. S. Brinen, W. S. Willett, C. S. Craik and R. J. Fletterick, *Biochemistry*, 1996, **35**, 5999-6009.
36 G. S. Jackson, I. Murray, L. L. P. Hosszu, N. Gibbs, J. P. Waltho, A. R. Clarke and J. Collinge, *PNAS*, 2001, **98**, 8531-8535.
37 D. R. Brown, K. Qin, J. W. Herms, A. Madlung, J. Manson, R. Strome, P. E. Fraser, T. Kruck, A. von Bohlen, W. Schulz-Schaeffer, A. Giese, D. Westaway and H. Kretzschmar, *Nature*, 1997, **390**, 684-687.
38 H. Zenga, D. S. Hwang, J. N. Israelachvilib and J. H. Waite, *PANS*, 2010, **107**, 12850-12853.
39 S. W. Taylor, G. W. Luther and J. H. Waite, *Inorg. Chem.*, 1994, **33**, 5819-5824.
40 J. C. G. Esteves da Silva, A. A. S. C. Machado, C. J. S. Oliveira and M. S. S. D. S. Pinto, *Talanta*, 1998, **45**,1155-1165.
41 H. Cao and Q. Liu, *J. Solution Chem.*, 2009, **38**, 1071-1077.
42 A. David, P. Kopečková, A. Rubinstein and J. Kopeček, *Bioconjugate Chem.*, 2001, **12**, 890-899.
43 A. David, P. Kopečková, J. Kopeček and A. Rubinstein, *Pharm. Res.*, 2002, **19**, 1114-1122
44 G. M. Hayes, P. E. Carrigan and L. J. Miller, *Cancer Res.*, 2007, **67**, 2072-2080.
45 J. -H. Mao, I. -J. Kim, D. Wu, J. Climent, H. C. Kang, R. DelRosario and A. Balmain, *Science*, 2008, **321**, 1499-1502.

Graphical Abstract

Protein-responsive assemblies from catechol-metal ion supramolecular coordination

A synergistic strategy combining the driving forces of both catechol-metal ion coordination and polymer self-assembly, can organize polymers into hybrid nanoassemblies with tunable morphologies and protein-triggered disassembly feature.